Report

Shaping Fission Yeast Cells by Rerouting Actin-Based Transport on Microtubules

Libera Lo Presti[1] and Sophie G. Martin[1,*]
[1]Department of Fundamental Microbiology, Faculty of Biology and Medicine, University of Lausanne, Biophore Building, 1015 Lausanne, Switzerland

Summary

Kinesins and myosins transport cargos to specific locations along microtubules and actin filaments, respectively. The relative contribution of the two transport systems for cell polarization varies extensively in different cell types, with some cells relying exclusively on actin-based transport while others mainly use microtubules. Using fission yeast, we asked whether one transport system can substitute for the other. In this organism, microtubules and actin cables both contribute to polarized growth by transporting cargos to cell poles, but with distinct roles: microtubules transport landmarks to label cell poles for growth and actin assembly but do not directly contribute to the growth process [1]. Actin cables serve as tracks for myosin V delivery of growth vesicles to cell poles [2–4]. We engineered a chimera between the motor domain of the kinesin 7 Tea2 and the globular tail of the myosin V Myo52, which we show transports Ypt3, a myosin cargo receptor, to cell poles along microtubules. Remarkably, this chimera restores polarized growth and viability to cells lacking actin cables. It also bypasses the normal microtubule-dependent marking of cell poles for polarized growth, but not for other functions. Thus, a synthetic motor protein successfully redirects cargos along a distinct cytoskeletal route.

Results and Discussion

We tested whether actin-based long-range transport could be transferred onto microtubules. To this aim, we constructed a chimeric protein containing the motor domain of the kinesin 7 Tea2 and the cargo-binding region of the myosin V Myo52, one of the two fission yeast myosin V motors and the only one required for polarized cell growth [3, 4]. This construct also contains the coiled-coil regions of both motor proteins to ensure correct folding and dimerization, separated by GFP (Figure 1A). We expressed this Tea2N-GFP-Myo52C fusion (hereafter referred to as kinesin-myosin chimera) as an integrated copy and performed most of our analysis in cells lacking functional actin cables as a consequence of the deletion of either all myosin V (*myo51Δ myo52Δ*, hereafter named *myoVΔ*) [3, 4] or the formin For3, responsible for actin cable assembly (*for3Δ*) [2, 5].

The kinesin motor domain was functional to travel along microtubules. The chimera localized to cell tips in wild-type, *myoVΔ*, and *for3Δ* cells. Treatment with methyl benzimidazole carbamate (MBC), a drug that depolymerizes microtubules, or use of a *mal3Δ* background, in which microtubule biogenesis is dramatically altered [6, 7], blocked cell tip accumulation,

whereas treatment with the actin-sequestering drug latrunculin A (LatA) had no effect (Figure 1B). Two-color imaging showed that the chimera moved with microtubules at a rate of 3.6 ± 1.3 μm/min (n = 25), similar to the rate of the Tea2 kinesin (Figure 1C; see also Movie S1 available online) [8, 9]. Faster-moving speckles (10.5 ± 3 μm/min, n = 20) were also observed, as is the case for endogenous Tea2 [9]. Thus, the kinesin-myosin chimera uses microtubules as tracks.

To test the functionality of the myosin cargo-binding domain, we first defined a bona fide cargo for Myo52, no examples of which have yet been described. In the budding yeast, the Rab11-family GTPases Ypt31p and Ypt32p contribute to the interaction of the myosin V Myo2p with post-Golgi vesicles [10–12]. The fission yeast homolog Ypt3 is required at multiple steps of the exocytic pathway, including at post-Golgi steps, and accumulates at cell poles [13]. We found that Ypt3 coimmunoprecipitated and partly colocalized with Myo52 in wild-type cells (Figures 2A and 2C). In contrast, Ypt3 failed to localize to cell tips in either *myo52Δ* cells or *for3Δ* cells lacking actin cables (Figure 2B). These data suggest that Ypt3 is a cargo receptor for Myo52. Although GFP-Ypt3 failed to localize to cell tips in *myoVΔ* cells, its localization to cell tips was restored upon expression of the kinesin-myosin chimera (Figure 2C; Figure S1). Ypt3 localization coincided with that of the chimera and became microtubule dependent. Thus, the kinesin-myosin chimera transports myosin cargos along microtubules to cell tips.

Remarkably, the kinesin-myosin chimera restored polarized cell growth to *myoVΔ* and *for3Δ* cells (Figure 3A and data not shown). This effect was microtubule dependent, because the kinesin-myosin chimera conferred no rescuing effect in a *mal3Δ* background. These cells rewired to transport growth vesicles along microtubules showed thinner, more pointed cell poles than wild-type cells transporting vesicles along actin cables, especially upon prolonged expression of the chimera, suggesting enhanced focusing of growth. This observation is in agreement with the localization of the cargo receptor Ypt3, which showed a more concentrated localization at cell poles when delivered by kinesin-myosin transport relative to wild-type cells (Figure 2C), suggesting that the zone of vesicle delivery dictates the width of the growth zone.

We investigated the organization of microtubules in *myoVΔ* and *myoVΔ* cells expressing the kinesin-myosin chimera. Cells lacking type V myosins displayed an abnormal microtubule cytoskeleton: they exhibited more microtubule bundles than wild-type strains (WT: 3.7 ± 1 bundles, n = 30 cells; *myoVΔ*: 4.7 ± 1.3 bundles, n = 46 cells), and microtubules were often disorganized, especially in rounder cells (Figure 3B). Abnormalities in microtubule cytoskeleton organization were also previously noted in *myo52Δ* cells and *for3Δ* cells [2, 14]. However, microtubule-delivered factors such as Tea1 or Tea4 were localized correctly to cell tips in *myoVΔ*, indicating that the global polarity of the microtubule network is preserved in this strain (data not shown). Upon expression of the kinesin-myosin chimera, microtubule bundle organization and number were restored to that of wild-type cells (3.8 ± 0.9 bundles, n = 38 cells; Figure 3B). Microtubule networks are known to self-organize within given space constraints. In *myoVΔ* cells

*Correspondence: sophie.martin@unil.ch

A Tea2N — Myo52C

Tea2N-GFP-myo52C

B

C Tea2N-GFP-Myo52C   mCherry-Atb2   Merge

expressing the kinesin-myosin chimera, microtubule-dependent targeting of growth components to cell poles may contribute to the remodeling of the microtubule network by promoting cell elongation. This would create a direct positive feedback between polarized growth and microtubule organization that may lead to the thinner appearance of cell tips in these rewired cells.

Fission yeast cells lacking functional actin cables are still partly polarization competent, because polarized exocytosis still occurs in these mutants. This is due to the cytoskeleton-independent localization of the exocyst complex at cell tips, which promotes vesicle tethering and polar secretion even in the absence of actin cables [15–17]. We thus tested whether the kinesin-myosin chimera could restore polarized cell growth to cells lacking both actin cables and a functional exocyst complex. Whereas double mutants of *for3Δ* with *exo70Δ*, a nonessential component of the exocyst, are sick and misshapen [15, 17], expression of the chimera promoted the formation of elongated cells (Figure 3C). In addition, the chimera also rescued the temperature-sensitive growth defect of *for3Δ* and *for3Δ exo70Δ* cells (Figures 3D and 3E). We were unable to confidently test this aspect in the *myoVΔ* cells as a result of the high rate of spontaneous suppressors in this strain. In summary, rerouting long-range actin-based transport onto microtubules bypasses the need for actin cables.

In these rewired cells, microtubules now have the dual function of marking cell poles for growth and delivering growth vesicles to these sites. We thus asked whether the landmark function had become dispensable. This function depends on the Tea1-Tea4 complex, which is normally transported to cell tips by the Tea2 kinesin and CLIP-170 Tip1 protein and anchored at the membrane by a prenylated anchor protein, Mod5 [8, 18–23]. The Tea1-Tea4 complex marks cell poles as sites of growth, in part by recruiting the formin For3 for actin cable assembly [19]. This complex also nucleates the formation of gradients of the kinase Pom1 from cell tips to regulate timing and positioning of cell division [21, 24, 25]. Cells mutant for *tea1* or *tea4* do not accurately position growth at cell tips, leading to the formation of curved or T-shaped cells [19–21]. They also localize the actin and growth machinery to only one single cell pole. *tea4Δ* cells expressing the kinesin-myosin fusion remained monopolar and the chimera localized to only one cell pole, probably as a result of dimerization with endogenous Myo52 (data not shown). We thus additionally deleted *myo52*. *tea4Δ myo52Δ* double-mutant cells, like *tea1Δ for3Δ* cells [26], are sick and misshapen. When these cells expressed the kinesin-myosin fusion, however, the chimera localized to both cell ends and restored rod shape (Figures 3F and 3G). These rewired *tea4Δ* cells also maintained their elongated shape upon recovery from stress and did not form T shapes, like the rounder *tea4Δ myo52Δ* or *tea1Δ for3Δ* double-mutant cells [26]. However, the chimera did not rescue the division defect of *tea4Δ myo52Δ* cells, which showed large numbers of often mispositioned septated and multiseptated cells, and failed to significantly rescue bipolar growth. The poor growth of these double mutants was also not improved. In summary, the long chain of events of microtubule delivery, cell tip

Figure 1. The Kinesin-Myosin Chimera Tea2N-GFP-Myo52C Moves along Microtubules to Cell Tips

(A) Schematic representation and predicted fold of the chimeric protein Tea2N-GFP-Myo52C.

(B) Localization of Tea2N-GFP-Myo52C in *myoVΔ* (left panels) and *for3Δ* (right panels) cells in the absence of any treatment, after 15 min 10 μM LatA treatment, after 30 min 25 μg/ml MBC treatment, and upon deletion

of *mal3*. Arrows point to tip localization of the chimera, which is lost upon microtubule disruption (MBC, *mal3Δ* cells) but not upon actin disruption (LatA).

(C) Tea2N-GFP-Myo52C dots (green, arrows) colocalize with microtubule bundles in a strain coexpressing mCherry-atb2 (red).

Scale bars represent 5 μm.
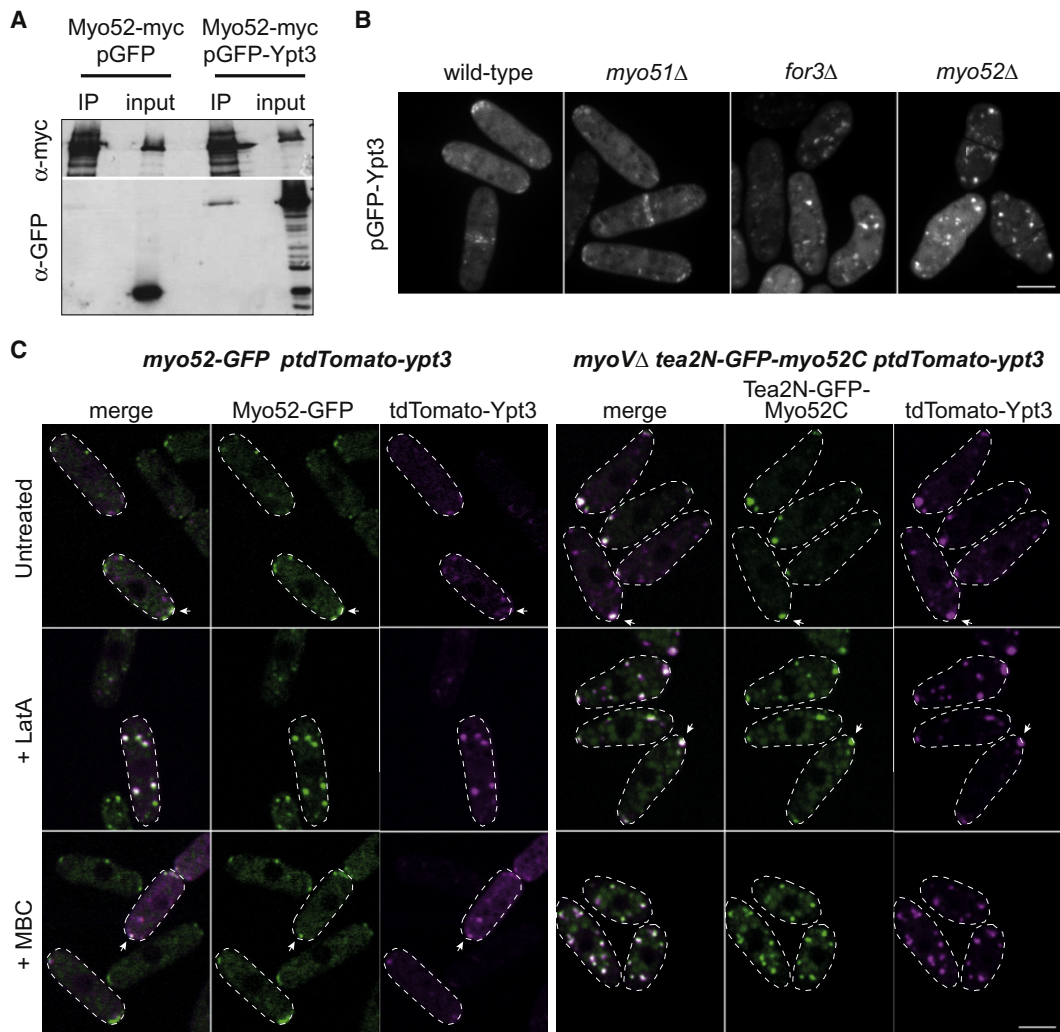
Figure 2. Ypt3 Is a Myo52 Cargo Receptor Localizing to Cell Tips and Is Rerouted along Microtubules by the Kinesin-Myosin Chimera

(A) GFP-Ypt3 coimmunoprecipitates with Myo52-myc. Extracts from *myo52-myc* cells transformed either with empty vector pREP41-GFP (left) or with pREP41-GFP-ypt3 (right) were immunoprecipitated with anti-myc antibodies and blotted with anti-GFP and anti-myc antibodies.

(B) Localization of GFP-Ypt3 expressed from plasmid in wild-type, *myo51Δ*, *myo52Δ*, and *for3Δ* cells.

(C) Wild-type cells expressing endogenous Myo52-GFP (left panels, green) and *myoVΔ* cells expressing Tea2N-GFP-Myo52C (right panels, green) transformed with pRep41-tdTomato-ypt3 (purple). Whereas Ypt3 dots localize at cell tips with Myo52 in an actin-dependent manner in wild-type cells (left), they localize to cell tips with chimera particles in a microtubule-dependent manner in rewired cells transporting Myo52 cargos along microtubules (right) (see also control strains in Figure S1). Colocalization of the two signals is shown in the merge channel by the white color. The only partial colocalization of Ypt3 with Myo52 in wild-type cells is due in part to the fast rate of Myo52 movement and the time delay between acquisition of the two colors. Accordingly, colocalization is more prominent when movements are prevented by LatA treatment. LatA and MBC were applied as indicated in Figure 1B. Scale bars represent 5 μm.

marking, actin cable assembly, and myosin transport can be collapsed into a single step by transporting myosin cargos along microtubules to achieve elongated cell shape. However, this simplified system is detrimental for other cellular events, in agreement with the idea that Tea4 plays roles in addition to marking cell ends for growth [24, 25].

These data provide several important insights about the function and plasticity of cytoskeletal systems. First, they describe a functional kinesin-myosin fusion. To our knowledge, this is the first such engineered chimeric motor protein. Interestingly, there is at least one natural precedent for this kind of chimera, where some plant kinesins harbor a MyTH4 domain typical of several myosin classes [27], indicating that domain exchange between myosins and kinesins may have occurred during evolution. Second, they demonstrate that in

fission yeast, actin cables probably have a single function— that of forming tracks for myosin V for polar secretion. This can be bypassed by transporting these cargos along an alternative cytoskeletal route. The temperature sensitivity of cells lacking actin cables is likely due to the inefficiency of polar secretion.

Finally, these data show that similar shapes can be achieved through distinct polarization strategies. Studies in multiple cell types have shown varied requirement for each cytoskeletal transport system. For instance, in budding yeast, cargo transport for polarized growth depends exclusively on myosin V walking along actin cables [28]. In contrast, other cells, such as neurons, melanocytes, and some filamentous fungi, rely largely on kinesins for long-range transport, and some of these cell types only hand cargos over to myosins for short-range
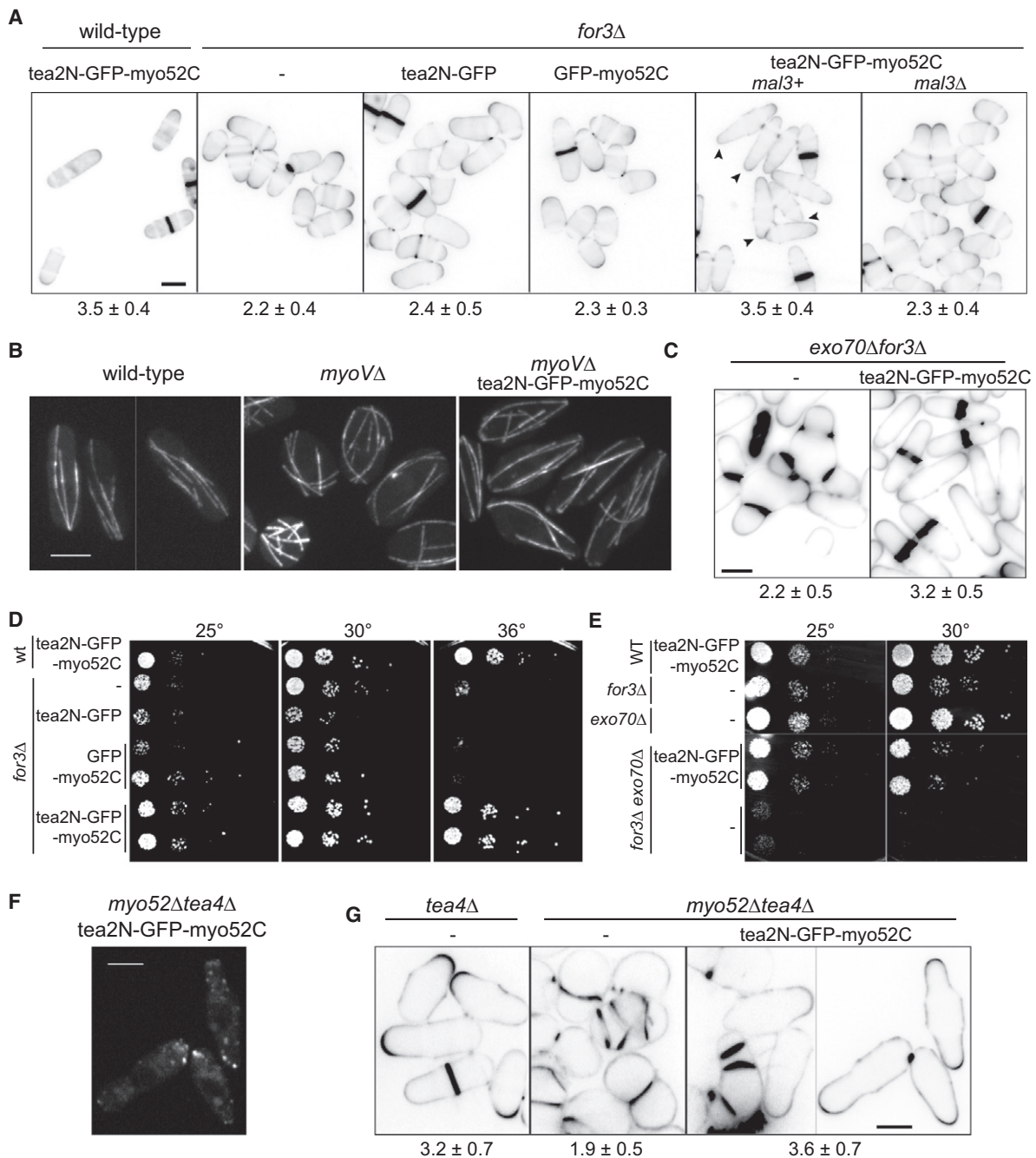
Figure 3. The Kinesin-Myosin Chimera Restores Shape and Growth to Cells Lacking Actin Cables

(A) Calcofluor staining of indicated genotypes. The chimera restores an elongated cell shape to *for3Δ* cells. This shape depends on microtubules, because it is abolished in *mal3Δ* background. Arrowheads point to a few repolarized cells with narrow cell poles. The numbers below each panel show the average ratio of cell length to cell width measured on septated cells (n = 30; standard deviation is indicated); high numbers indicate elongated shapes.

(B) Microtubule organization in wild-type, *myoVΔ*, and *myoVΔ* cells expressing the kinesin-myosin chimera, as labeled by GFP-Atb2.

(C) Calcofluor staining and measurements as in (A), showing restoration of elongated shape by the chimera in *for3Δ exo70Δ* cells.

(D) The kinesin-myosin chimera rescues the temperature-sensitive growth defect of *for3Δ* cells. The panel shows growth dilution assays of wild-type cells expressing the kinesin-myosin chimera, *for3Δ* cells, and *for3Δ* cells expressing either the chimera or control constructs. Plates were incubated at the indicated temperature for 3 days.

(E) Growth dilution assay of wild-type cells expressing the chimera and *for3Δ*, *exo70Δ*, and *for3Δ exo70Δ* cells expressing or not expressing the chimera. Plates were incubated at the indicated temperature for 4 days.

(F) Localization of Tea2N-GFP-Myo52C in *myo52Δ tea4Δ* cells.

(G) Calcofluor staining to show the change in cell shape induced by expression of the chimera in *myo52Δ tea4Δ* cells. Genotypes are indicated above the images. Note that whereas the kinesin-myosin chimera restores shape to *myo52Δ tea4Δ* cells (rightmost panel), it fails to correct (second panel from right) the multiseptation defect of the double mutant (second panel from left). Measurements are as in (A). Note that the high ratio for the *myo52Δ tea4Δ* cells expressing the chimera may be an overestimation due to reinitiation of growth before completion of cytokinesis.

Inverted images are shown for (A), (C), and (G). Scale bars represent 5 μm.

peripheral distribution [29–31]. Actin filaments and microtubules can also show extensive interactions [32], suggesting cooperativity or redundancy for transport. Although this diversity indicates the exquisite adaptation of cytoskeletal arrangements to each cell type, it also shows, at evolutionary timescales, the high versatility of the transport systems. Our approach demonstrates that a single cell is plastic enough to allow use of different tracks for cargo transport to the same cellular location. Thus, the destination, rather than the tracks, is what matters most for polarized cell growth. Whereas evolution has led to highly buffered systems providing robustness for cell polarization, our simple synthetic biology approach to rewiring long-range transport demonstrates that these systems can be simplified to achieve similar cell shape.

Experimental Procedures

Strains, Growth Conditions, and Pharmacological Treatments

Standard genetic methods and growth conditions were used. Cells were grown in Edinburgh minimal media (EMM) supplemented with appropriate amino acids (ALU) or YE5S as indicated. Particular care was taken to avoid accumulation of suppressors in poorly growing strains by backcrossing, rapid stocking of newly generated strains, and streaking them freshly at each experiment.

For growth dilution assays, chimera expression was induced by growth in EMM-AL lacking thiamine for 16–17 hr at 30°C. Cultures were then diluted in EMM-AL to a final optical density of 0.05, and 1/10 serial dilutions were spotted on YE5S, which contains thiamine but allows low basal expression of the *nmt* promoter.

Methyl benzimidazole carbamate (MBC, Sigma) was used at a final concentration of 25 μg/ml from a stock of 2.5 mg/ml in DMSO. MBC treatment was performed for 30 min at 30°C unless otherwise indicated.

Latrunculin A (LatA; Phillip Crews, University of California, Santa Cruz) was used from a stock of 20 mM in DMSO at a final concentration of 10 μM to disrupt cables and a final concentration of 200 μM to disassemble all actin structures. LatA treatment was performed at either 25°C or 30°C, unless otherwise indicated, for 15 or 5 min for the doses indicated above, respectively. Both doses disrupted Myo52 localization to cell tips, whereas neither dose had any effect on the localization of the kinesin-myosin chimera.

Molecular Biology Methods

All plasmids were constructed using standard molecular biology techniques. In general, genes or gene fragments were cloned after PCR using as template genomic DNA or plasmids and primers containing 5′ extensions with specific restriction sites. Details of the primers and restriction sites used are available upon request.

Functionality of tdTomato-ypt3 was assessed by the ability of plasmid pRep41-tdTomato-ypt3 to rescue the temperature-sensitive growth defect of *ypt3-i5*.

The tea2N-GFP-myo52C cassette was cloned under control of the weak thiamine-repressible *nmt* promoter in pRIP82 vector and encodes, in this order, amino acids 1–557 of Tea2 (indicated as Tea2N; UniProtKB accession number Q1MTQ1), a ASSGRA linker, GFP, a GS linker, and amino acids 926–1516 of Myo52 (Myo52C; UniProtKB accession number O94477). The linearized vector was integrated into the *ura4* genomic locus. Integrative plasmids pRip82-tea2N-GFP and pRip82GFP-myo52C were constructed in parallel as controls and integrated with an identical strategy.

Microscopy

Microscopy was performed with either a spinning-disk confocal microscope or a wide-field fluorescence microscope. Calcofluor (Sigma) was added at a final concentration of 5 μg/ml from a 200× stock solution. Images in Figure 3A were acquired on a wide-field Leica AF6000 system consisting of a DM6000B upright microscope fitted with a 40×/0.75 NA objective, a Leica DFC350x CCD camera, a Leica EL6000 light source, and Chroma filter sets. Images were acquired with Leica LAS AF software. Images in Figure 3C were acquired on DeltaVision system composed of a customized Olympus IX-71 inverted microscope stand fitted with a Plan Apo 60×/1.42 NA oil objective, a CoolSNAP HQ2 camera, and an Insight SSI 7 color combined unit illuminator. Images were acquired with softWoRx software.

All other images were acquired on a spinning-disk confocal microscope consisting of a Leica DMI4000B inverted microscope equipped with an HCX PL APO 100×/1.46 NA oil objective and a PerkinElmer Ultraview confocal system (including a Yokagawa CSU22 real-time confocal scanning head, an argon/krypton laser, and a cooled 14-bit frame transfer EMCCD C9100-50 camera). Stacks of z series confocal sections were acquired at 0.3 μm intervals with Ultraview or Volocity software, and images were rendered by 2D maximum-intensity projection unless otherwise indicated. For imaging and quantification of GFP-tagged constructs and Ypt3-tdTomato dynamics, images were acquired in single focal planes with 1–1.4 s exposure and maximum-speed interval time for a total of 60 s.

Figures were prepared with Adobe Photoshop Elements 6 and Adobe Illustrator CS3, and movies were prepared with ImageJ 1.41.

All length and width measurements were performed on Calcofluor-stained septated cells with the "Measure" tool in ImageJ 1.41. The average ratio of cell length to cell width was then calculated with Microsoft Excel.

Biochemical Methods

Strains for coimmunoprecipitation were obtained by transformation with pREP41-GFP-ypt3 [13] or empty plasmids. Extracts from yeast grown in EMM-AU medium for 21 hr at 30°C were prepared in CXS buffer (50 mM HEPES [pH 7.0], 20 mM KCl, 1 mM MgCl$_2$, 2 mM EDTA[pH 7.5], and protease inhibitor cocktail) by grinding in liquid nitrogen with a mortar and pestle. After thawing, NaCl and Triton X-100 were added to final concentrations of 150 mM and 0.1% respectively. For immunoprecipitations, 150 μl soluble extract was added to 20 μl sheep anti-mouse magnetic Dynabead slurry (Dynal) prebound to 2 μg monoclonal anti-Myc antibodies (9E10, Santa Cruz) and incubated for 2 hr at 4°C. Magnetic Dynabeads were then washed four times in CXS 0.1% Triton X-100 and three times in IPP150 (150 mM Tris [pH 8.0], 150 mM NaCl, 0.1% Nonidet P40, 2 mM EDTA, 1 mM MgCl$_2$). Immunoprecipitated material was then recovered by boiling Dynabeads in 60 μl SDS sample buffer for 5 min at 95°C. Standard protocols were used for SDS-PAGE and western blot analysis. Antibodies used on western blots were mouse monoclonal anti-myc (9E10, Santa Cruz) and a home-made rabbit polyclonal anti-GFP.

Supplemental Information

Supplemental Information includes one figure and one table and can be found with this article online at doi:10.1016/j.cub.2011.10.033.

References

1. Martin, S.G. (2009). Microtubule-dependent cell morphogenesis in the fission yeast. Trends Cell Biol. *19*, 447–454.
2. Feierbach, B., and Chang, F. (2001). Roles of the fission yeast formin for3p in cell polarity, actin cable formation and symmetric cell division. Curr. Biol. *11*, 1656–1665.
3. Motegi, F., Arai, R., and Mabuchi, I. (2001). Identification of two type V myosins in fission yeast, one of which functions in polarized cell growth and moves rapidly in the cell. Mol. Biol. Cell *12*, 1367–1380.
4. Win, T.Z., Gachet, Y., Mulvihill, D.P., May, K.M., and Hyams, J.S. (2001). Two type V myosins with non-overlapping functions in the fission yeast Schizosaccharomyces pombe: Myo52 is concerned with growth polarity and cytokinesis, Myo51 is a component of the cytokinetic actin ring. J. Cell Sci. *114*, 69–79.
5. Nakano, K., Imai, J., Arai, R., Toh-E, A., Matsui, Y., and Mabuchi, I. (2002). The small GTPase Rho3 and the diaphanous/formin For3 function in polarized cell growth in fission yeast. J. Cell Sci. *115*, 4629–4639.

6. Beinhauer, J.D., Hagan, I.M., Hegemann, J.H., and Fleig, U. (1997). Mal3, the fission yeast homologue of the human APC-interacting protein EB-1 is required for microtubule integrity and the maintenance of cell form. J. Cell Biol. *139*, 717–728.

7. Busch, K.E., and Brunner, D. (2004). The microtubule plus end-tracking proteins mal3p and tip1p cooperate for cell-end targeting of interphase microtubules. Curr. Biol. *14*, 548–559.

8. Browning, H., Hackney, D.D., and Nurse, P. (2003). Targeted movement of cell end factors in fission yeast. Nat. Cell Biol. *5*, 812–818.

9. Busch, K.E., Hayles, J., Nurse, P., and Brunner, D. (2004). Tea2p kinesin is involved in spatial microtubule organization by transporting tip1p on microtubules. Dev. Cell *6*, 831–843.

10. Casavola, E.C., Catucci, A., Bielli, P., Di Pentima, A., Porcu, G., Pennestri, M., Cicero, D.O., and Ragnini-Wilson, A. (2008). Ypt32p and Mlc1p bind within the vesicle binding region of the class V myosin Myo2p globular tail domain. Mol. Microbiol. *67*, 1051–1066.

11. Lipatova, Z., Tokarev, A.A., Jin, Y., Mulholland, J., Weisman, L.S., and Segev, N. (2008). Direct interaction between a myosin V motor and the Rab GTPases Ypt31/32 is required for polarized secretion. Mol. Biol. Cell *19*, 4177–4187.

12. Santiago-Tirado, F.H., Legesse-Miller, A., Schott, D., and Bretscher, A. (2011). PI4P and Rab inputs collaborate in myosin-V-dependent transport of secretory compartments in yeast. Dev. Cell *20*, 47–59.

13. Cheng, H., Sugiura, R., Wu, W., Fujita, M., Lu, Y., Sio, S.O., Kawai, R., Takegawa, K., Shuntoh, H., and Kuno, T. (2002). Role of the Rab GTP-binding protein Ypt3 in the fission yeast exocytic pathway and its connection to calcineurin function. Mol. Biol. Cell *13*, 2963–2976.

14. Martín-García, R., and Mulvihill, D.P. (2009). Myosin V spatially regulates microtubule dynamics and promotes the ubiquitin-dependent degradation of the fission yeast CLIP-170 homologue, Tip1. J. Cell Sci. *122*, 3862–3872.

15. Bendezú, F.O., and Martin, S.G. (2011). Actin cables and the exocyst form two independent morphogenesis pathways in the fission yeast. Mol. Biol. Cell *22*, 44–53.

16. Nakano, K., Toya, M., Yoneda, A., Asami, Y., Yamashita, A., Kamasawa, N., Osumi, M., and Yamamoto, M. (2011). Pob1 ensures cylindrical cell shape by coupling two distinct rho signaling events during secretory vesicle targeting. Traffic *12*, 726–739.

17. Snaith, H.A., Thompson, J., Yates, J.R., 3rd, and Sawin, K.E. (2011). Characterization of Mug33 reveals complementary roles for actin cable-dependent transport and exocyst regulators in fission yeast exocytosis. J. Cell Sci. *124*, 2187–2199.

18. Browning, H., Hayles, J., Mata, J., Aveline, L., Nurse, P., and McIntosh, J.R. (2000). Tea2p is a kinesin-like protein required to generate polarized growth in fission yeast. J. Cell Biol. *151*, 15–28.

19. Martin, S.G., McDonald, W.H., Yates, J.R., 3rd, and Chang, F. (2005). Tea4p links microtubule plus ends with the formin for3p in the establishment of cell polarity. Dev. Cell *8*, 479–491.

20. Mata, J., and Nurse, P. (1997). tea1 and the microtubular cytoskeleton are important for generating global spatial order within the fission yeast cell. Cell *89*, 939–949.

21. Tatebe, H., Shimada, K., Uzawa, S., Morigasaki, S., and Shiozaki, K. (2005). Wsh3/Tea4 is a novel cell-end factor essential for bipolar distribution of Tea1 and protects cell polarity under environmental stress in S. pombe. Curr. Biol. *15*, 1006–1015.

22. Snaith, H.A., and Sawin, K.E. (2003). Fission yeast mod5p regulates polarized growth through anchoring of tea1p at cell tips. Nature *423*, 647–651.

23. Brunner, D., and Nurse, P. (2000). CLIP170-like tip1p spatially organizes microtubular dynamics in fission yeast. Cell *102*, 695–704.

24. Hachet, O., Berthelot-Grosjean, M., Kokkoris, K., Vincenzetti, V., Moosbrugger, J., and Martin, S.G. (2011). A phosphorylation cycle shapes gradients of the DYRK family kinase Pom1 at the plasma membrane. Cell *145*, 1116–1128.

25. Huang, Y., Chew, T.G., Ge, W., and Balasubramanian, M.K. (2007). Polarity determinants Tea1p, Tea4p, and Pom1p inhibit division-septum assembly at cell ends in fission yeast. Dev. Cell *12*, 987–996.

26. Feierbach, B., Verde, F., and Chang, F. (2004). Regulation of a formin complex by the microtubule plus end protein tea1p. J. Cell Biol. *165*, 697–707.

27. Richards, T.A., and Cavalier-Smith, T. (2005). Myosin domain evolution and the primary divergence of eukaryotes. Nature *436*, 1113–1118.

28. Pruyne, D., Legesse-Miller, A., Gao, L., Dong, Y., and Bretscher, A. (2004). Mechanisms of polarized growth and organelle segregation in yeast. Annu. Rev. Cell Dev. Biol. *20*, 559–591.

29. Aspengren, S., Hedberg, D., Sköld, H.N., and Wallin, M. (2009). New insights into melanosome transport in vertebrate pigment cells. Int. Rev. Cell Mol. Biol. *272*, 245–302.

30. Steinberg, G., and Perez-Martin, J. (2008). Ustilago maydis, a new fungal model system for cell biology. Trends Cell Biol. *18*, 61–67.

31. Hirokawa, N., Niwa, S., and Tanaka, Y. (2010). Molecular motors in neurons: transport mechanisms and roles in brain function, development, and disease. Neuron *68*, 610–638.

32. Rodriguez, O.C., Schaefer, A.W., Mandato, C.A., Forscher, P., Bement, W.M., and Waterman-Storer, C.M. (2003). Conserved microtubule-actin interactions in cell movement and morphogenesis. Nat. Cell Biol. *5*, 599–609.

Supplemental Information

Shaping Fission Yeast Cells by Rerouting

Actin-Based Transport on Microtubules

Libera Lo Presti and Sophie G. Martin
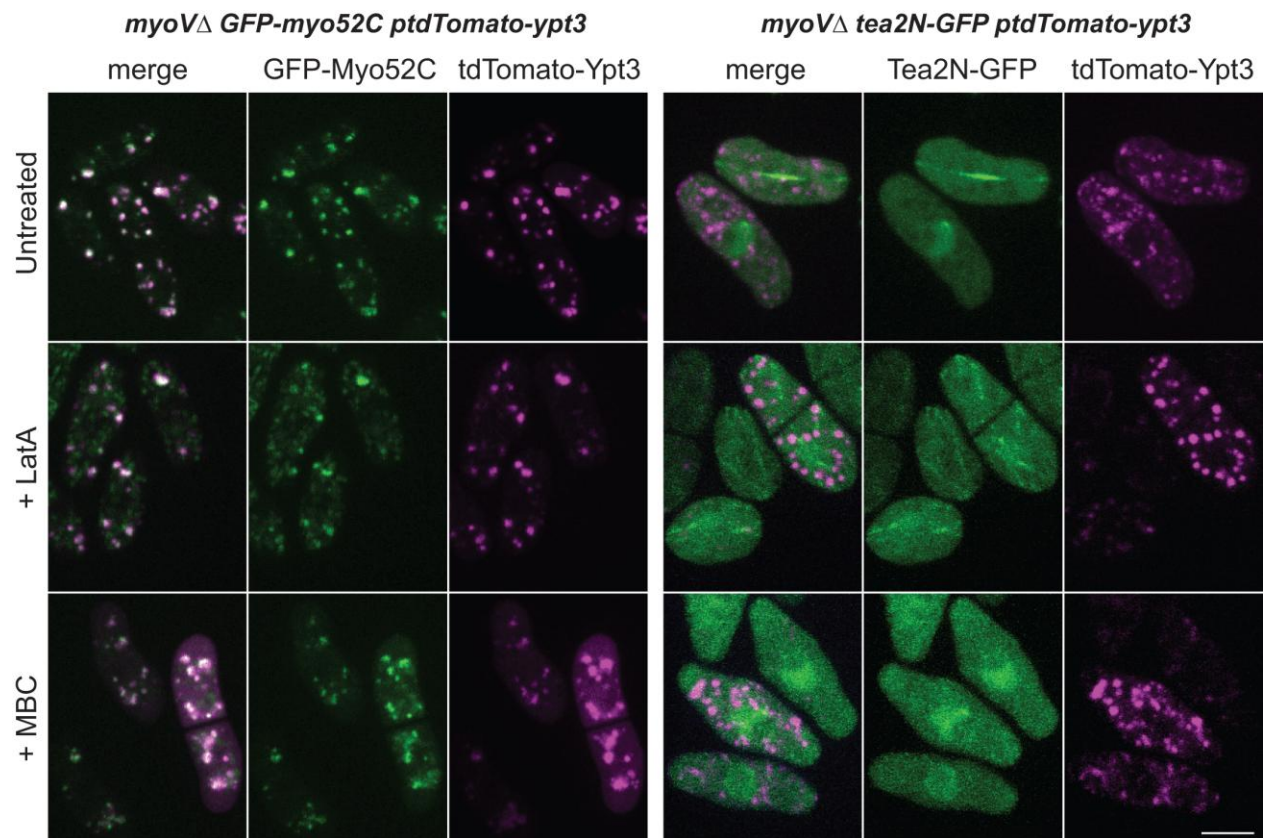
Figure S1. Controls for the Kinesin-Myosin Chimera

Images of *myoVΔ* cells expressing either GFP-Myo52C (left panels; green) or Tea2N-GFP (right panels; green) transformed with pRep41-Tomato-ypt3 (purple). Ypt3 particles fail to localize at cell tips in both strains, indicating that Tea2N motor and Myo52C tail are by themselves not sufficient to target Ypt3 to cell tips. Note the colocalization of Myo52C and Ypt3, shown by the white color in the merge channel. LatA and MBC were applied as indicated in Figure 1B. Scale bar represents 5 μm.

Table S1. Strains Used in This Study

Strain	Genotype	Source
YSM106	*myo52-GFP::kanMX ade6- leu1-32 ura4-D18*	Lab stock
YSM1071	*h- myo52-myc-kanMX ade6-M216 leu1-32 ura4-D18*	Lab stock
YSM1056	*h+ for3::kanMX6 ade6- leu1-32 ura4-D18*	[2]
YSM1182	*h+ ade6-M216 leu1-32 ura4-D18*	Lab stock
YSM1532	*h- myo51::ura4+ ade6-M216 leu1-32 ura4-D18*	[4]
YSM1923	*h- myo52:.ura4+ leu1-32 ura4-294*	[4]
YSM1545	*myo52::ura4+ myo51:ura4+ ade6-M216 leu1-32 ura4-D18*	This study
YSM1924	*for3::kanMX ura4+ leu1-32*	This study
YSM1925	*h- leu1-32 ura4-294::tea2N-GFP-myo52C-ura4+*	This study
YSM1926	*myo52::ura4+ myo51::ura4+ leu1-32 ura4-294::tea2N-GFP-ura4+*	This study
YSM1927	*myo52::ura4+ myo51::ura4+ leu1-32 ura4-294::GFP-myo52C-ura4+*	This study
YSM1928	*mal3::his3+ myo52::ura4+ myo51::ura4+ leu1-32 ura4-294::tea2N-GFP-myo52C-ura4+*	This study
YSM1929	*myo52::ura4+ myo51::ura4+ leu1-32 ura4-294::tea2N-GFP-myo52C-ura4+*	This study
YSM1930	*for3::kanMX leu1-32 ura4-294::tea2N-GFP-myo52C-ura4+*	This study
YSM1931	*for3::kanMX leu1-32 ura4-294::GFP-myo52C-ura4+*	This study
YSM1932	*for3::kanMX leu1-32 ura4-294::tea2N-GFP-ura4+*	This study
YSM1933	*mal3::his3+ for3::kanMX leu1-32 ura4-294::tea2N-GFP-myo52C-ura4+*	This study
YSM1742	*h+ exo70::natMX ade6- leu1-32 ura4-D18*	[15]
YSM1934	*for3::KanMX exo70::natMX leu1-32 ura4-294::tea2N-GFP-myo52C-ura4+*	This study
YSM1935	*for3::KanMX exo70::natMX ura4- leu1-32*	This study
YSM992	*myo52:.ura4+ tea4::kanMX ura4-D18 leu1-32*	Lab stock
YSM1936	*myo52:.ura4+ tea4::kanMX leu1-32 ura4-294::tea2N-GFP-myo52C-ura4+*	This study
YSM1937	*myo52::ura4+ myo51::ura4+ aur::mCherry-atb2 leu1-32 ura4-294::tea2N-GFP-myo52C-ura4+*	This study
YSM332	*tea4::kanMX ura4-D18 leu1-32*	[19]
YSM1960	*h+ leu1-32::pSV40-GFP-atb2(leu1+) ade6- leu1-32 ura4-D18*	Lab stock
YSM1961	*h+ leu1-32::pSV40-GFP-atb2(leu1+) myo52::ura4+ myo51::ura4+ ura4-D18 leu1-32*	This study
YSM1962	*h+ leu1-32::pSV40-GFP-atb2(leu1+) myo52::ura4+ myo51::ura4+ ura4-294::tea2N-GFP-myo52C-ura4+ leu1-32*	This study